

Photophoresis on particles hotter/colder than the ambient gas for the entire range of pressures

C. Loesche, T. Husmann

Fakultät für Physik, Universität Duisburg-Essen, Lotharstr. 1, 47048 Duisburg, Germany

Abstract

Small, illuminated aerosol particles embedded in a gas experience a photophoretic force. Most approximations assume the mean particle surface temperature to be effectively the gas temperature. This might not always be the case. If the particle temperature or the thermal radiation field strongly differs from the gas temperature (optically thin gases), given approximations for the free molecule regime overestimate the photophoretic force by an order of magnitude on average and for individual configurations up to three magnitudes. We apply the radiative equilibrium condition from the previous paper (Paper 1) — where photophoresis in the free molecular flow regime was treated — to the slip flow regime. The slip-flow model accounts for thermal creep, frictional and thermal stress gas slippage and temperature jump at the gas-particle interface. In the limiting case for vanishing Knudsen numbers — the continuum limit — our derived formula has a mean error of only 4 % compared to numerical values. Eventually, we propose an equation for photophoretic forces for all Knudsen numbers following the basic idea from Rohatschek by interpolating between the free molecular flow and the continuum limit.

Keywords: photophoresis; rarefied gas; aerosols; transition regime; black body; thermal radiation

1. INTRODUCTION

Illuminated particles suspended in a gas experience photophoretic forces Yalamov et al. (1976a,b); Rohatschek (1995); Loesche et al. (2013). For directed illumination like in Fig. 1, a simple description for high Knudsen numbers is based on a kinetic description of the momentum transfer between impinging gas molecules and the particles, which is stronger on one particular side of the particles. Often this is related to a temperature gradient across the particles' surface which leads to a motion away from the radiation source.

Several experiments show photophoresis (Wurm & Krauss 2008; Loesche et al. 2014; van Eymeren & Wurm 2012) and the theoretical treatment of photophoretic forces in different pressure regimes has also progressed (Malai et al. 2012b; Beresnev et al. 1993; Yalamov et al. 1976a,b; Reed 1977).

The findings in the first paper (Loesche et al. 2016), (hereafter referred to as Paper 1) are based on work by Hidy & Brock (1967); Tong (1973); Yalamov et al. (1976a), which allow only low radiative fluxes I and small gas-particle temperature differences. It presented a new free molecular flow (fm) approximation, that now also supports the case of considerably higher radiative fluxes (I) and hotter/lower surface temperatures with respect to the surrounding gas (T_∞), while assuming the particle to be in equilibrium with an external radiation field at T_{rad} . It also performs very well for particles of low thermal conductivity k which so far only Yalamov et al. (1976a) does, too. Paper 1 showed, that the optimized linearizations used have an excellent effect on the results, reducing the minimum and maximum relative error of the analytical equation (within the model) to $\approx -50\%$ and 7% , respectively.

Beresnev et al. (1993); Chernyak & Beresnev (1993) proposed an advanced kinetic model for high Knudsen numbers, where also thermal radiation was considered. The external radiation field was at the temperature of the gas. For the fm limit they also provide a handy equation, that is similar to the one in Paper 1. However, the model only allowed small radiative fluxes I and therefore only small temperature difference between gas and particle.

Conversely, for low Knudsen numbers, especially in the slip-flow (sf) regime, there are hydrodynamic models proposed by Yalamov et al. (1976b); Reed (1977); Mackowski (1989), where the first work also treats evaporation. None of these models allow high intensities I and also do not account for thermal radiation. For high intensities and temperature deviance of gas and particle Malai et al. (2012a,b) already proposed a model, incorporating thermal radiation and temperature dependent heat conductivities of gas $k_g(T)$ and particle $k(T)$ as well as gas viscosity $\eta(T)$. Like in Beresnev et al. (1993), the radiation field is at the temperature of the gas.

In this paper, we apply the findings from Paper 1 on other Knudsen regimes with the aim to find an accurate but handy interpolation function for the entire range of pressures. This interpolation also supports higher intensities, and therefore the mean particle surface temperature to differ from the gas temperature T_∞ . Furthermore, it also includes the temperature of the radiation field T_{rad} , which is not necessarily the gas temperature, depending on the setting. The interpolation is based on approximations for the free molecular fm and continuum (co) limits following the findings of Hettner (1928); Rohatschek (1995). However, as we have two temperatures, i.e. T_∞ and T_{rad} , which

do not necessarily have to be the same, we propose another *sf* model in Section 3. From the equation for the *sf* regime we obtain the limiting case for vanishing Knudsen numbers (*co*). In the *sf* regime we account for thermal creep, frictional and thermal stress gas slippage and temperature jump at the gas-particle interface. We will not include temperature dependent k , k_g and η but show how to account for that in Section 5. For smaller particles the boundary conditions in the *sf* regime can also be extended by some additional addends which are linear in the Knudsen number (Malai et al. 2012b), introducing several more parameters. However, as mentioned before, we interpolate between the *co* and *fm* approximations. Therefore we do not incorporate too many Knudsen-number dependent boundary conditions into this model which vanish in the limiting case $Kn \rightarrow 0$ (*co*). A discussion of the results and a comparison to other models is done in Section 5.

All variables in this paper are also listed in Tab. A.4, including some basic relations. Section A provides some additional information for the interested reader in the supplementaries.

2. CLARIFICATION/KNUDSEN REGIMES

The Knudsen number Kn is defined as the ratio of the mean free path of the gas molecules/atoms λ and the characteristic length of the problem r_0 (here this is the particle radius)

$$Kn = \frac{\lambda}{r_0}. \quad (1)$$

The *fm* and *co* regimes are the limits $Kn \rightarrow \infty$ and $Kn \rightarrow 0$, respectively. For fixed characteristic particle sizes r_0 , both limits basically infer $p \rightarrow 0$ and $p \rightarrow \infty$, respectively. For high Knudsen numbers, the photophoretic force is linear in p (Paper 1). Conversely, for low Knudsen numbers, the force goes with p^{-1} (this paper). That means, for both limits it is $\lim_{Kn \rightarrow \infty} F_{\text{phot}}(p) = \lim_{Kn \rightarrow 0} F_{\text{phot}}(p) = 0$. This is obviously not useful. Our considerations made in the *fm* and *co* regimes are hence for large and small enough Knudsen numbers, respectively.

Technically, $Kn \geq 10$ is associated with the *fm* regime, the transition regime is assumed for a Knudsen number range between $0.25 \lesssim Kn \lesssim 10$, but the lower bound varies with different transfer processes on particles (Hidy & Brock 1970). For low Knudsen numbers $Kn \ll 1$, the *co* regime is extended with a slip-flow boundary condition. This sub-regime is called the slip-flow regime. Here, no general bounds can be provided (Hidy & Brock 1970). A sketch of the different regimes is appended in Fig. A.6.

Therefore it is more exact to say, the considerations made in the *co* regime are actually made in the *sf* regime and only the limiting case for vanishing Knudsen numbers is associated with the *co* regime. On the other hand, as *fm* photophoresis is not meant for zero pressure ($Kn \neq 0$), one can also talk about *co* photophoresis ($Kn \neq \infty$).

3. PHOTOPHORESIS AT LOW KNUDSEN NUMBERS

For solid particles at low Knudsen numbers (e.g. large aerosols) the photophoretic force is a direct result of thermal

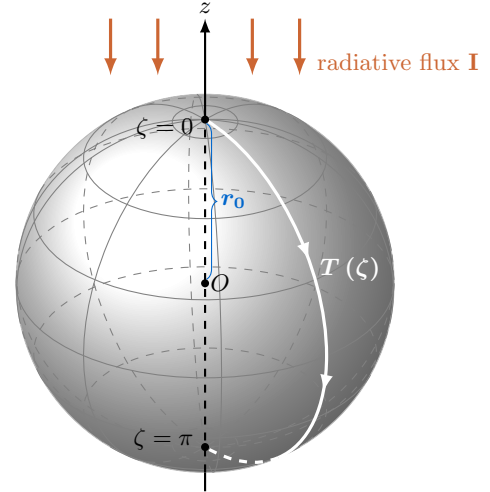


Figure 1: Visualization of the situation considered. Illumination is directed along z -axis, thus for a homogeneous particle the surface temperature only depends on ζ (spherical coordinate system (r, ζ, ξ)). The sphere's radius is r_0 . The temperature of the gas is T_∞ ($r \rightarrow \infty$), the temperature of the radiation field is T_{rad} .

creep along a surface ∂V of the suspended particle (Reed 1977; Bakanov 2004), which occurs in case of a temperature gradient in the gas, which is tangential to ∂V .

For directed illumination of a homogeneous, spherical particle embedded in an effectively infinite gas as shown in Fig. 1, an equation for the ensuing *longitudinal* photophoretic force at low Knudsen numbers is proposed. The particle is supposed to be in a radiative equilibrium with an external radiation field at temperature T_{rad} . This radiation field can also be emitted by the gas itself, which has the temperature T_∞ far away from the suspended particle. We present two means to describe photophoresis for directed illumination at a radiative flux of I . One is solely for the slip-flow regime with the limiting case of $Kn \rightarrow \infty$ (*co*) and the second one interpolates between all regimes, using the *co* limit and the *fm* limit from Paper 1.

The model consists of a hydrodynamic part and a heat transfer part. In this setting (Fig. 1), both problems are axisymmetric in ξ , i.e. they only depend on the coordinates r and ζ . The z -axis is therefore set parallel to the direction of illumination and motion at speed u , and especially: $\mathbf{e}_z = -\mathbf{e}_I$. Gases and fluids with a small dynamic viscosity can be treated as ideal fluids. Additionally, if the fluid is incompressible and the flow is free of vortices, the flow can be treated like a potential flow. However, this statement is right for almost every point in the fluid except at the particle-fluid interface. Friction will definitely contribute here, large flow speed gradients occur, and friction forces will be comparable to inertial forces. Therefore, the boundary conditions in this model account for thermal creep as well as frictional and thermal stress gas slippage at the gas-particle interface.

Before setting up the hydrodynamic model, we give a short insight into thermal creep.

3.1. Thermal creep

Thermal creep causes a gas flow tangential to a surface (tangent \mathbf{t} , normal \mathbf{n}) at a mass speed v which obeys the equation (Brenner 2009)

$$(\mathbb{1} - \mathbf{n} \otimes \mathbf{n}) \cdot (\mathbf{v} - \mathbf{u}) = \kappa_s \eta_{\text{kin}} (\mathbb{1} - \mathbf{n} \otimes \mathbf{n}) \cdot \nabla \log T_g \quad \text{on } \partial V. \quad (2)$$

The mass velocity \mathbf{v} obeys the continuity equation

$$\frac{\partial \rho}{\partial t} + \nabla \cdot \rho \mathbf{v} = 0 \quad \text{on } \partial V, \quad (3)$$

\mathbf{u} is the velocity of the surface ∂V relative to the gas, η_{kin} denotes the kinematic viscosity of the gas, and ρ and T_g the gas mass density and gas temperature, respectively (Brenner 2005). κ_s is the thermal creep coefficient (also thermal slip coefficient)¹. Brenner (2009) points out, that various experts on molecular dynamics agree on the correctness of this equation for gases, even though the underlying gas-kinetic molecular theory is not rigorous but only semi-quantitative.

The original value of the thermal creep coefficient $\kappa_s = \frac{3}{4}$ goes back to Maxwell (1879). Bakanov (1992) lists a couple of parameters a_{κ_s} and b_{κ_s} for different models which relate κ_s and the momentum accommodation coefficient α_m by the equation

$$\kappa_s(\alpha_m) \simeq \frac{3}{4} (a_{\kappa_s} + b_{\kappa_s} \alpha_m), \quad (4)$$

where a_{κ_s} is close to 1 and b_{κ_s} around 0.5, thus the thermal creep coefficient can be expected to obtain values between $0.75 \leq \kappa_s \leq 1.24$. Rohatschek (1995) assumes a value of $\kappa_s = 1.14$ for $\alpha_m = 0.9$ and this value is also used by Loesche et al. (2014); Hesse (2011). Ivchenko et al. (1993) also suggested a model with more accurate values for κ_s . One of the latest works is Ivchenko et al. (2007).

3.2. Hydrodynamic model

The momentum balance in the fluid is given by

$$\rho \frac{d\mathbf{v}}{dt} \equiv \rho \left(\frac{\partial \mathbf{v}}{\partial t} + (\mathbf{v} \cdot \nabla) \mathbf{v} \right) = -\nabla p + \nabla \cdot \underline{\sigma} + \rho \mathbf{F}_{\text{ext}}, \quad (5)$$

where $\underline{\sigma}$ denotes the stress tensor, that is related to the friction tensor $\underline{\mathbf{R}}$ ²

$$\sigma_{ik} = -p \delta_{ik} + R_{ik} \quad (6a)$$

$$R_{ik} = \eta_{\text{dyn}} \left(\frac{\partial v_i}{\partial x_k} + \frac{\partial v_k}{\partial x_i} \right) - \delta_{ik} \frac{2}{3} \eta_{\text{dyn}} \nabla \cdot \mathbf{v}. \quad (6b)$$

¹Brenner (2006, 2009) also proposed a nonmolecular thermodynamic theory of thermal creep, based on a hydrodynamic theory, that is valid for physiochemically and thermally inert solids suspended in not only gases but also fluids as

$$(\mathbb{1} - \mathbf{n} \otimes \mathbf{n}) \cdot (\mathbf{v}_m - \mathbf{u}) = D \gamma_{\text{exp}} (\mathbb{1} - \mathbf{n} \otimes \mathbf{n}) \cdot \nabla T_g \quad \text{on } \partial V,$$

introducing the fluid's self-diffusion coefficient D and the fluid's thermal expansion coefficient (at constant pressure) $\gamma_{\text{exp}} = -\frac{1}{\rho} \left(\frac{\partial \rho}{\partial T_g} \right)_p$. In contrast to this equation, Eq. 2 is only valid for gases and no restrictions on the solids are imposed.

²Inserting Eq. 6 into Eq. 5 yields the Navier-Stokes equation

$$\rho \left(\frac{\partial \mathbf{v}}{\partial t} + (\mathbf{v} \cdot \nabla) \mathbf{v} \right) = -\nabla p + \eta_{\text{dyn}} \Delta \mathbf{v} + \frac{1}{3} \eta_{\text{dyn}} \nabla (\nabla \cdot \mathbf{v}) + \rho \mathbf{F}_{\text{ext}}.$$

The photophoretic motion of the particle causes the gas to move at small Reynolds numbers Re , hence the convective acceleration $(\mathbf{v} \cdot \nabla) \mathbf{v}$ can be omitted (vortex-free fluid: $\nabla \times \mathbf{v} = 0$). Furthermore, we want to get the quasi-stationary solution ($\partial_t \mathbf{v} = 0$) for the incompressible fluid (source-free velocity field $\nabla \cdot \mathbf{v} = 0 \Rightarrow \partial_t \rho = 0$). Eventually, we have no body force ($\mathbf{F}_{\text{ext}} = 0$). Therefore Eq. 5 simplifies to

$$\nabla p = \eta_{\text{dyn}} \Delta \mathbf{v}. \quad (7)$$

Because of $\nabla \times \mathbf{v} = 0$, \mathbf{v} has a scalar potential ($\nabla \times \nabla f = 0$ for a scalar function f). Also, because of $\nabla \cdot \mathbf{v} = 0$, \mathbf{v} has a vector potential, generally written as Ψ .

Considering the symmetry of the three-dimensional problem, the fluid/gas velocity is

$$\mathbf{v} = v_r \mathbf{e}_r + v_\zeta \mathbf{e}_\zeta, \quad (8)$$

and therefore quasi-two-dimensional.

3.2.1. Ansatz

In orthogonal coordinates q_1, q_2, q_3 (with the accompanying scaling factors h_1, h_2, h_3) a three-dimensional, stationary flow of an incompressible Newtonian fluid with symmetry in q_3 has a vector potential that only depends on two variables $\Psi = \Psi(q_1, q_2)$. Therefore it can be set $\Psi \sim \psi \mathbf{e}_3$, and the velocity can subsequently be written as

$$\mathbf{v} = \nabla \times \Psi \quad (9a)$$

$$= -\nabla \times \left(\psi \frac{\mathbf{e}_3}{h_3} \right) \quad (9b)$$

$$= \frac{\mathbf{e}_3}{h_3} \times \nabla \psi(q_1, q_2) - \psi(q_1, q_2) \nabla \times \frac{\mathbf{e}_3}{h_3} \quad (9c)$$

$$= \frac{\mathbf{e}_3}{h_3} \times \nabla \psi(q_1, q_2). \quad (9d)$$

ψ is called the Stokes stream function. Applying $\mathbf{e}_3 \times \nabla$ on Eq. 7 (and using Eq. 9d) yields the equation that ψ satisfies, that is also the governing equation for the flow (Schubert 2015)

$$E^4 \psi = 0 \quad (10a)$$

$$E^2 = \frac{h_3}{h_1 h_2} \left[\frac{\partial}{\partial q_1} \left(\frac{h_2}{h_1 h_3} \frac{\partial}{\partial q_1} \right) + \frac{\partial}{\partial q_2} \left(\frac{h_1}{h_2 h_3} \frac{\partial}{\partial q_2} \right) \right]. \quad (10b)$$

In spherical coordinates (r, ζ, ξ) the scaling factors are $(h_1, h_2, h_3) = (1, r, r \sin \zeta)$, and hence it is $E^2 = \partial_{r,r} + \frac{\sin \zeta}{r^2} \partial_\zeta \left(\frac{1}{\sin \zeta} \partial_\zeta \right)$. The velocity subsequently reads

$$\mathbf{v} = \begin{pmatrix} v_r \\ v_\zeta \\ v_\xi \end{pmatrix} = \frac{1}{r \sin \zeta} \begin{pmatrix} -\frac{1}{r} \partial_\zeta \psi \\ \partial_r \psi \\ 0 \end{pmatrix}. \quad (11)$$

The ansatz for ψ is (Reed 1977)

$$\psi(r, \zeta) = u \psi_R(r) \psi_Z(\zeta) \quad (12a)$$

$$\psi_Z(\zeta) = \frac{1}{2} \sin^2 \zeta. \quad (12b)$$

The radial part $\psi_R(r)$ is determined by the governing equation $E^4 \psi = 0$, which formulates an ordinary differential equation for $\psi_R(r)$. Its solution is

$$\psi_R(r) = \frac{a}{r} + br + cr^2 + dr^4. \quad (13)$$

In the following, the gas temperature is expanded into a Legendre series

$$T_g(r, \zeta) = T_\infty + \sum_{v=0}^{\infty} C_v \left(\frac{r_0}{r}\right)^{v+1} P_v(\cos \zeta). \quad (14)$$

3.2.2. Boundary conditions

Like in Reed (1977), we use an inertial reference frame at rest with the fluid far away from the particle (Eq. 18c), where the z -axis is parallel to the direction of illumination (due to symmetry in ξ , see Fig. 1). The fluid does not penetrate the particles surface, therefore the fluid velocity has no additional normal component than $u \cos \zeta$ (Eq. 18a). The thermal creep introduces a (tangential) boundary condition with symmetry in ξ , given by Eq. 1. To be able to use orthogonality relations, Eq. 1 is linearized at the mean near-surface temperature of the gas ³ ($\eta_{\text{kin}} = \eta_{\text{dyn}}/\rho$)

$$v_t \simeq \kappa_s \frac{\eta_{\text{dyn}}}{\rho r_0 T_g|_{\partial V}} \frac{\partial T_g}{\partial \zeta} \Big|_{r=r_0}, \quad (15)$$

where $\frac{\partial T_g}{\partial t} \Big|_{\partial V} = \frac{1}{r_0} \frac{\partial T_g}{\partial \zeta} \Big|_{r=r_0}$. As the friction forces are strong at the particle-gas interface, we account for shear stress, in spherical coordinates given as

$$R_{\zeta r} = \eta_{\text{dyn}} \left(\frac{1}{r} \frac{\partial v_r}{\partial \zeta} + r \frac{\partial}{\partial r} \left(\frac{v_\zeta}{r} \right) \right), \quad (16)$$

and thermal stress (Chang & Keh 2012)

$$\sigma_t = -\frac{\eta_{\text{dyn}}^2}{\rho T_g|_{\partial V}} \left(\frac{1}{r} \frac{\partial^2 T}{\partial r \partial \zeta} - \frac{1}{r^2} \frac{\partial T}{\partial \zeta} \right). \quad (17)$$

Summarizing, the boundary conditions are given as (Reed 1977; Chang & Keh 2012)

$$v_r = u \cos \zeta \quad \text{on } \partial V \quad (18a)$$

$$v_\zeta = -u \sin \zeta + v_t + \frac{\kappa_m K n r_0}{\eta_{\text{dyn}}} (\sigma_{\zeta r} + \kappa_h \sigma_t) \quad \text{on } \partial V \quad (18b)$$

$$v_r \xrightarrow{r \rightarrow \infty} 0, \quad v_\zeta \xrightarrow{r \rightarrow \infty} 0. \quad (18c)$$

The values for the thermal stress slip coefficient κ_h vary between 1 and 3 (Chang & Keh 2012); κ_m is the gas-kinetic frictional slip which is related to the momentum accommodation coefficient α_m , with values around $1.00 \leq \kappa_m \leq 1.35$ and typically taking about 1.25 (Reed 1977).

³ $(\mathbb{1} - \mathbf{n} \otimes \mathbf{n}) \cdot \mathbf{u} = \begin{pmatrix} 0 \\ u_\zeta \\ u_\xi \end{pmatrix}$ with $u_\zeta = -u \sin \zeta$ and $u_\xi = 0$ is separately put in the boundary condition Eq. 18b as not only \mathbf{u} but other addends occur, too.

3.2.3. Solution

The velocity $\mathbf{v} = v_r \mathbf{e}_r + v_\zeta \mathbf{e}_\zeta$ is completely given by Eqs. 11–14, and the unknown parameters a, b, c and d are restricted by the boundary conditions. From Eq. 18c, it can be concluded that

$$c = d = 0. \quad (19)$$

Because of Eq. 18a, it is

$$a + r_0^2 (b + r_0) = 0. \quad (20)$$

Eq. 18b involves a derivation of the Legendre series of the gas temperature in ζ (Eq. 14). As it is $\partial_\zeta P_v(\cos \zeta) = P_v^1(\cos \zeta)$, only the polynomials P_v^1 occur in Eq. 18b. All terms with u and a, b are linear in $\sin \zeta = P_1^1(\cos \zeta)$. As pairwise different P_v^1 are orthogonal to each other (see Eq. A.1 in the appendix for details), a scalar product of this boundary condition with P_v^1 will isolate the interesting addends containing a and b . Together with Eq. 20 it is

$$a = \frac{r_0^3}{1 + 3\kappa_m K n} \left(\frac{1}{2} + (\kappa_s + 3\kappa_h \kappa_m K n) \frac{\eta_{\text{dyn}}}{\rho r_0 T_g|_{\partial V} u} C_1 \right) \quad (21a)$$

$$b = -\frac{r_0}{1 + 3\kappa_m K n} \left(\frac{1}{2} + (\kappa_s + 3\kappa_h \kappa_m K n) \frac{\eta_{\text{dyn}}}{\rho r_0 T_g|_{\partial V} u} C_1 \right) - r_0, \quad (21b)$$

and subsequently

$$v_r = \frac{\cos \zeta r_0^2}{2\rho T_g|_{\partial V} r^3} \frac{2C_1 \eta_{\text{dyn}} \left(1 + \frac{r^2}{r_0^2}\right) (\kappa_s + 3\kappa_h \kappa_m K n)}{1 + 3\kappa_m K n}. \quad (22a)$$

$$\frac{\rho r_0 T_g|_{\partial V} u \left(1 + 3\frac{r^2}{r_0^2} (1 + 2\kappa_m K n)\right)}{1 + 3\kappa_m K n}. \quad (22b)$$

$$v_\zeta = \frac{\sin \zeta r_0^2}{4\rho T_g|_{\partial V} r^3} \frac{2C_1 \eta_{\text{dyn}} \left(1 - \frac{r^2}{r_0^2}\right) (\kappa_s + 3\kappa_h \kappa_m K n)}{1 + 3\kappa_m K n}. \quad (22c)$$

$$\frac{\rho r_0 T_g|_{\partial V} u \left(1 - 3\frac{r^2}{r_0^2} (1 + 2\kappa_m K n)\right)}{1 + 3\kappa_m K n}. \quad (22d)$$

Here, due to the symmetry of the setting, only F_z is not zero (Happel & Brenner 1983):

$$F_z = -8\pi \eta_{\text{dyn}} \lim_{r \rightarrow \infty} \frac{r \psi(r, \zeta)}{r^2 \sin^2 \zeta} \quad (23)$$

$$= -4\pi \eta_{\text{dyn}} u b. \quad (24)$$

Inserting v_r and v_ζ into Eq. 24 yields the force as

$$F_z = -4\pi \frac{\eta_{\text{dyn}}^2}{\rho T_g|_{\partial V}} \frac{\kappa_s + 3\kappa_h \kappa_m K n}{1 + 3\kappa_m K n} C_1 - 6\pi \eta_{\text{dyn}} r_0 u \frac{1 + 2\kappa_m K n}{1 + 3\kappa_m K n}. \quad (25)$$

In the steady state, where the particle moves at constant speed u , it is $F_z = 0$. That means, two forces are compensate each

other, that is the photophoretic force

$$\mathbf{F}_{\text{phot}} = -4\pi \frac{\eta_{\text{dyn}}^2}{\rho T_{\text{g}}|_{\partial V}} \frac{\kappa_s + 3\kappa_h \kappa_m Kn}{1 + 3\kappa_m Kn} C_1 \mathbf{e}_z \quad (26)$$

and the drag/resistance force

$$\mathbf{F}_{\text{drag}} = -6\pi \eta_{\text{dyn}} r_0 \frac{1 + 2\kappa_m Kn}{1 + 3\kappa_m Kn} \mathbf{u}_{\text{phot}}. \quad (27)$$

The ensuing steady state velocity is

$$\mathbf{u}_{\text{phot}} = -\frac{2}{3} \frac{\eta_{\text{dyn}}}{\rho T_{\text{g}}|_{\partial V} r_0} \frac{\kappa_s + 3\kappa_h \kappa_m Kn}{1 + 2\kappa_m Kn} C_1 \mathbf{e}_z. \quad (28)$$

Instead of this equation, the Millikan drag equation can be used here, which is more accurate for $Kn \approx 1$ (Mackowski 1989).

In the following section, the unknown expansion coefficient C_1 of the gas temperature is determined by solving a heat transfer problem.

3.3. Heat transfer model

We follow the assumptions made in Paper 1, the particle is heated by directed illumination, which is described by the inhomogeneity $I q(r, \cos \zeta)$ in the heat transfer equation. The heat transfer model supports energy exchange with the gas, thermal radiation and a temperature jump at the gas-particle interface. The gas is supposed to be at temperature T_∞ far away from the suspended particle. The particle is required to be in radiative equilibrium with an external radiation field at temperature T_{rad} . This can also be the gas itself as $T_{\text{rad}} = T_\infty$.

3.3.1. Ansatz

The Péclet number Pe (Eq. A.3) is required to be small, then thermal diffusive transport predominates advective transport. Therefore the governing equations are

$$k \Delta T = -I q(r, \cos \zeta) \quad (29a)$$

$$k_{\text{g}} \Delta T_{\text{g}} = 0, \quad (29b)$$

for the particle and gas, respectively. $I = \varepsilon I_0$ is the absorbed radiative flux, ε denotes the emissivity⁴.

The ansatz for the particle temperature T is constructed insofar that on the surface it is given by the simple equation

$$T(r_0, \zeta) = \sum_{\nu=0}^{\infty} A_\nu P_\nu(\cos \zeta). \quad (30)$$

⁴In standard form $q(r, \zeta)$ is (Yalamov et al. 1976b; Malai et al. 2012a)

$$q(r, \zeta) = 2\chi_1 \chi_2 k_0 B(r, \zeta) \\ B(r, \zeta) = \frac{1}{2\pi} \int_0^{2\pi} \frac{|E(r, \zeta, \xi)|}{E_0^2} d\xi,$$

where $\chi = \chi_1 + i\chi_2$ is the complex refractive index and k_0 the wave number of an electromagnetic wave at amplitude E_0 .

For the general solution $T(r, \zeta) = T_1(r, \zeta) + T_2(r, \zeta)$, the homogeneous and particular ansatz functions are

$$T_1(r, \zeta) = \sum_{\nu=0}^{\infty} (A_\nu - B_\nu J_\nu(r_0)) \left(\frac{r}{r_0}\right)^\nu P_\nu(\cos \zeta) \quad (31a)$$

$$T_2(r, \zeta) = \sum_{\nu=0}^{\infty} B_\nu J_\nu(r) P_\nu(\cos \zeta). \quad (31b)$$

Then, $T_1 + T_2$ yield Eq. 30 on the surface. The particular solution employs the asymmetry factor J_ν

$$J_\nu(r) = \frac{1}{r_0} \left[r^{-\nu-1} \int_0^r s^{\nu+2} q_\nu(s) ds + r^\nu \int_r^{r_0} s^{\nu-1} q_\nu(s) ds \right] \quad (32a)$$

$$q_\nu(r) = \frac{2\nu+1}{2} \int_{-1}^1 q(r, x) P_\nu(x) dx \quad (32b)$$

$$J_\nu \equiv J_\nu(r_0) = \int_0^{r_0} \left(\frac{r}{r_0}\right)^{\nu+2} q_\nu(r) dr. \quad (32c)$$

$q_\nu(r)$ are the Legendre expansion coefficients of the source $q(r, \zeta)$. For perfectly absorbing spheres, the asymmetry factors yield $J_0 = 1/4$ and $J_1 = \pm 1/2$ (positive for irradiation into direction $\mathbf{e}_r = -\mathbf{e}_z$).

3.3.2. Boundary conditions

To account for thermal radiation and a temperature jump at the surface, the following boundary conditions were chosen

$$k \frac{\partial T}{\partial \mathbf{n}} = k_{\text{g}} \frac{\partial T_{\text{g}}}{\partial \mathbf{n}} - \sigma_{\text{SB}} \varepsilon (T^4 - T_{\text{rad}}^4) \quad \text{at } \partial V \quad (33a)$$

$$T_{\text{g}} - T = \kappa_t r_0 Kn \frac{\partial T_{\text{g}}}{\partial \mathbf{n}} \quad \text{at } \partial V \quad (33b)$$

$$T_{\text{g}} \xrightarrow{r \rightarrow \infty} T_\infty. \quad (33c)$$

The last boundary condition is already met by the ansatz for the gas temperature in Eq. 14. To prevent nonlinear mixing of the expansion coefficients A_ν and B_ν at multiple orders in the first boundary condition, the term $\sigma_{\text{SB}} \varepsilon (T^4 - T_{\text{rad}}^4)$ will be linearized at the mean temperature \tilde{T}

$$\sigma_{\text{SB}} \varepsilon (T^4 - T_{\text{rad}}^4) = \sigma_{\text{SB}} \varepsilon (4T \tilde{T}^3 - T_{\text{rad}}^4 - 3\tilde{T}^4) + \dots \quad (34)$$

$$\tilde{T} = \left(\frac{1}{4\pi} \int_0^{2\pi} \int_0^\pi T(\zeta)^4 \sin \zeta d\zeta d\xi \right)^{1/4}, \quad (35)$$

which is given by integrating the boundary conditions. The second boundary condition is the temperature jump condition at the gas-particle surface. For $Kn \rightarrow 0$ (*co* regime) the sphere and the gas layer surrounding it are in thermal equilibrium. The thermal accommodation coefficient α defines the temperature jump coefficient κ_t as Reed (1977)

$$\kappa_t(\alpha) \simeq \frac{15}{8} \left(\frac{1-\alpha}{\alpha} \right). \quad (36)$$

3.3.3. Solution

In a similar procedure as in Paper 1 the coefficients A and C can be obtained from the boundary conditions in Eqs. 33a and 33b by using the orthogonality relations of the Legendre polynomials $P_\nu = P_\nu^0$ (Eq. A.1), B is obtained by the inhomogeneous heat transfer equation (Eq. 29a; upper index sf means slip flow)

$$A_\nu^{\text{sf}} = \frac{I J_\nu}{\nu \frac{k}{r_0} + \frac{k_g}{r_0} \frac{\nu+1}{1+(\nu+1)\kappa_1 Kn} + 4\sigma_{\text{SB}}\varepsilon (\tilde{T}^{\text{sf}})^3} \quad \nu \geq 1 \quad (37a)$$

$$A_0^{\text{sf}} = \frac{I J_0 + \frac{1}{1+\kappa_1 Kn} \frac{k_g}{r_0} T_\infty + \sigma_{\text{SB}}\varepsilon \left(3 (\tilde{T}^{\text{sf}})^4 + T_{\text{rad}}^4\right)}{\frac{k_g}{r_0} \frac{1}{1+\kappa_1 Kn} + 4\sigma_{\text{SB}}\varepsilon (\tilde{T}^{\text{sf}})^3} \stackrel{\text{Eq. 38}}{=} \bar{T} \quad (37b)$$

$$B_\nu^{\text{sf}} = \frac{I r_0}{(2\nu+1)k} \quad (37c)$$

$$C_\nu^{\text{sf}} = \frac{1}{1+(\nu+1)\kappa_1 Kn} A_\nu^{\text{sf}} \quad \nu \geq 1 \quad (37d)$$

$$C_0^{\text{sf}} = \frac{1}{1+\kappa_1 Kn} \frac{I J_0 - 4\sigma_{\text{SB}}\varepsilon (\tilde{T}^{\text{sf}})^3 T_\infty + \sigma_{\text{SB}}\varepsilon \left(3 (\tilde{T}^{\text{sf}})^4 + T_{\text{rad}}^4\right)}{\frac{k_g}{r_0} \frac{1}{1+\kappa_1 Kn} + 4\sigma_{\text{SB}}\varepsilon (\tilde{T}^{\text{sf}})^3} \quad (37e)$$

3.3.4. Mean temperatures

The mean surface temperature \bar{T} is solely determined by the 0-th expansion coefficient (using Eq. A.1)

$$\bar{T} = \frac{1}{4\pi} \int_0^{2\pi} \int_0^\pi T(r_0, \zeta) \sin \zeta \, d\zeta \, d\xi \stackrel{\text{Eq. 30}}{=} A_0 \quad (38)$$

For the gas, the mean temperature across a spherical layer is given by

$$\overline{T_g(r)} = \frac{1}{4\pi} \int_0^{2\pi} \int_0^\pi T_g(r, \zeta) \sin \zeta \, d\zeta \, d\xi \stackrel{\text{Eq. 14}}{=} T_\infty + C_0^{\text{sf}} \frac{r_0}{r}, \quad (39)$$

and therefore the mean gas temperature around the particle is

$$\overline{T_g|_{\partial V}} = \overline{T_g(r_0)} = T_\infty + C_0^{\text{sf}}. \quad (40)$$

\tilde{T} can be obtained by integrating the boundary condition Eq. 33a around the sphere, and using Gauss's theorem

$$\begin{aligned} -k \int_{\partial V} \nabla T \cdot d\mathbf{A} &= \int_{\partial V} (k_g \mathbf{n} \cdot \nabla T + \sigma_{\text{SB}}\varepsilon (T^4 - T_{\text{rad}}^4)) \, dA \\ &= -k \int_V \Delta T \, dV \\ &\stackrel{\text{Eq. 29}}{=} \varepsilon I_0 \int_V q(r, \zeta) \, dV = \pi r_0^2 \varepsilon I_0. \end{aligned} \quad (41)$$

Then, the temperature \tilde{T} (Eq. 35) meets the balance

$$\pi r_0^2 \varepsilon I_0 = 4\pi r_0^2 \sigma_{\text{SB}}\varepsilon (\tilde{T}^4 - T_{\text{rad}}^4), \quad (42)$$

and is

$$\tilde{T}^{\text{sf}} = T_{\text{bb}} := \sqrt[4]{\frac{I_0}{4\sigma_{\text{SB}}} + T_{\text{rad}}^4}. \quad (43)$$

Inserted into Eq. 37a (A_1^{sf}), the photophoretic force $F^{\text{sf}} = F^{\text{sf}}(A_1^{\text{sf}})$ will become slightly non-linear in the radiative flux I_0 .

3.4. Result

Summarizing all previous findings, the photophoretic force in the slip flow regime with a gas temperature T_∞ and a radiation field temperature T_{rad} is given as

$$\mathbf{F}_{\text{phot}}^{\text{sf}} = -4\pi \frac{\eta_{\text{dyn}}^2}{\rho T_g|_{\partial V}} \frac{\kappa_s + 3\kappa_h \kappa_m Kn}{1 + 3\kappa_m Kn} \cdot \frac{1}{1 + 2\kappa_1 Kn \frac{k}{r_0} + \frac{k_g}{r_0} \frac{2}{1+2\kappa_1 Kn} + 4\sigma_{\text{SB}}\varepsilon T_{\text{bb}}^3} \mathbf{e}_z \quad (44a)$$

$$\overline{T_g|_{\partial V}} = T_\infty + \frac{1}{1 + \kappa_1 Kn} \frac{I J_0 - 4\sigma_{\text{SB}}\varepsilon T_{\text{bb}}^3 T_\infty + \sigma_{\text{SB}}\varepsilon (3 T_{\text{bb}}^4 + T_{\text{rad}}^4)}{\frac{k_g}{r_0} \frac{1}{1+\kappa_1 Kn} + 4\sigma_{\text{SB}}\varepsilon T_{\text{bb}}^3} \quad (44b)$$

$$T_{\text{bb}} = \sqrt[4]{\frac{I_0}{4\sigma_{\text{SB}}} + T_{\text{rad}}^4}. \quad (44c)$$

Apart from the additional radiative term $4\sigma_{\text{SB}}\varepsilon T_{\text{bb}}^3$, the results are in agreement with Eq. 36 from Reed (1977)⁵ and Eq. 29 from Mackowski (1989) for $\kappa_h = 0$.

Eventually, the photophoretic velocity is given as (Eq. 28)

$$\mathbf{u}_{\text{phot}}^{\text{sf}} = -\frac{2}{3} \frac{\eta_{\text{dyn}}}{\rho T_g|_{\partial V} r_0} \frac{\kappa_s + 3\kappa_h \kappa_m Kn}{1 + 2\kappa_m Kn} \cdot \frac{1}{1 + 2\kappa_1 Kn \frac{k}{r_0} + \frac{k_g}{r_0} \frac{2}{1+2\kappa_1 Kn} + 4\sigma_{\text{SB}}\varepsilon T_{\text{bb}}^3} \mathbf{e}_z. \quad (45)$$

3.5. Continuum limit

The rotationally symmetric solution above (Eq. 44) is reused to describe the force in the *co* limit ($Kn \rightarrow 0$). From the boundary condition Eq. 33c it is $T_g|_{\partial V} = \bar{T}$ at the surface, and therefore the force reads

$$\mathbf{F}_{\text{phot}}^{\text{co}} \stackrel{\text{Eq. 44a}}{=} -4\pi \kappa_s \frac{\eta_{\text{dyn}}^2}{\rho \bar{T}} \frac{I J_1}{\frac{k}{r_0} + 2\frac{k_g}{r_0} + 4\sigma_{\text{SB}}\varepsilon T_{\text{bb}}^3} \mathbf{e}_z \quad (46a)$$

$$\bar{T} \stackrel{\text{Eq. 40}}{=} T_\infty + \lim_{Kn \rightarrow 0} C_0^{\text{sf}} \quad (46b)$$

$$\begin{aligned} &= T_\infty + \frac{I J_0 - 4\sigma_{\text{SB}}\varepsilon T_{\text{bb}}^3 T_\infty + \sigma_{\text{SB}}\varepsilon (3 T_{\text{bb}}^4 + T_{\text{rad}}^4)}{\frac{k_g}{r_0} + 4\sigma_{\text{SB}}\varepsilon T_{\text{bb}}^3} \\ &\stackrel{\text{Eq. 38}}{=} \lim_{Kn \rightarrow 0} A_0^{\text{sf}} = \frac{I J_0 + \frac{k_g}{r_0} T_\infty + \sigma_{\text{SB}}\varepsilon (3 T_{\text{bb}}^4 + T_{\text{rad}}^4)}{\frac{k_g}{r_0} + 4\sigma_{\text{SB}}\varepsilon T_{\text{bb}}^3}. \end{aligned} \quad (46c)$$

⁵Reed (1977) incorporates the radiation source term into the boundary condition, with $J_1 = 1/2$.

The photophoretic velocity is

$$\mathbf{u}_{\text{phot}}^{\text{co}} \stackrel{\text{Eq. 45}}{=} -\frac{2}{3} \kappa_s \frac{\eta_{\text{dyn}}}{\rho \bar{T} r_0} \frac{I J_1}{\frac{k}{r_0} + 2\frac{k_g}{r_0} + 4\sigma_{\text{SB}} \varepsilon T_{\text{bb}}^3} \mathbf{e}_z. \quad (47)$$

4. INTERPOLATING BETWEEN *fm*- AND *co*-PHOTOPHORESIS

An empirical method is used to describe the photophoretic force in the transition regime due to the complexity of transport processes in this regime. Rohatschek (1995) presents a phenomenological equation satisfying the linear proportionality of the force with the pressure in the *fm* regime and the inverse proportionality in the *co* regime by

$$\frac{F_{\text{phot}}}{\hat{F}} = \frac{2 + \delta}{\frac{p}{\hat{p}} + \delta + \frac{\hat{p}}{p}}, \quad (48)$$

with the free parameter δ to be adjusted along the experimental values (Fig. 2). Because of the changing proportionality at an unknown pressure \hat{p} , the force peaks at $\hat{F} = F(\hat{p})$. Hettner (1928) already suggests the same equation with $\delta = 0$. Rohatschek (1995) also favors it, justifying it to be the best-fitting version of conducted experiments in the past, including work of other researchers such as Tong (1975); Arnold & Amani (1980). Nonetheless, the experiments of Rosen & Orr (1964) with large carbon agglomerates do not obey above's law. Rohatschek (1985) gave evidence that for large agglomerates, theories of ΔT -photophoresis cannot be applied because of the superposition of $\Delta\alpha$ - and ΔT -photophoresis. One of the experimental results mentioned by Rohatschek (1995) implied $\delta = 0.8$. The gas-kinetic calculations made by Chernyak & Beresnev (1993) suggested $\delta \simeq 1$, and for slip-flow theories, e.g. in Reed (1977) it is even $\delta \geq 2$, both fitting about 67% and less than 50%, respectively, of the experimental findings Rohatschek (1995) discussed.

Hettner (1928) suggested an interpolation (Eq. 20 in the respective publication), which is

$$\frac{1}{F_{\text{phot}}} = \frac{1}{F_{\text{phot}}^{\text{co}}} + \frac{1}{F_{\text{phot}}^{\text{fm}}}. \quad (49)$$

We therefore present a new interpolation along Rohatschek (1995) for $\delta = 0$, whose scope of validity includes not only $|\bar{T}/T_\infty| \simeq 1$ but also stronger temperature deviations and therefore higher intensities. This interpolation is based on the *fm* equation from Paper 1 and the *co* equation from this paper (Eq. 46).

4.1. Longitudinal photophoresis in the transition regime

To determine \hat{F} and \hat{p} for longitudinal photophoresis in the description of Eq. 48 for $\delta = 0$, a few more steps have to be made. Starting with Eq. 49, the force in the *fm* and the *co* regimes is ($A_0^{\text{co}} := \lim_{k \rightarrow 0} A_0^{\text{sf}}$ etc., $A_\nu^{\text{co}} \equiv C_\nu^{\text{co}}$, $A_1^{\text{fm}} =$

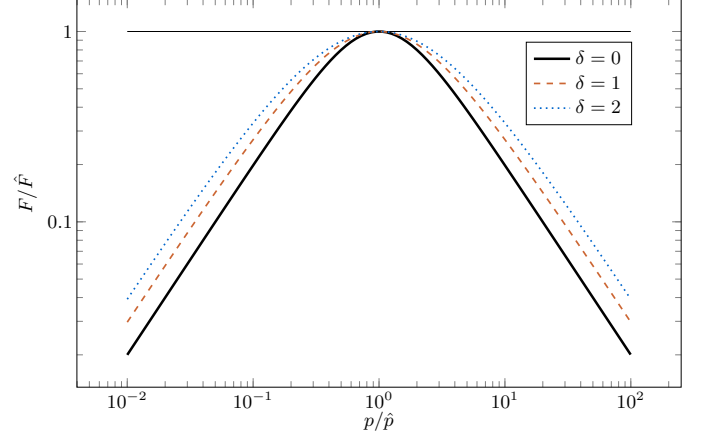


Figure 2: Interpolation between *fm* and *co* regimes. The photophoretic force peaks at $\hat{F} = F(\hat{p})$.

$\frac{I J_1}{\frac{k}{r_0} + h + 4\sigma_{\text{SB}} \varepsilon (\tilde{T}^{\text{fm}})^3}$ (Paper 1), and changing the notation used in Paper 1 from T_g^\ominus to T_∞)

$$F_{\text{phot}}^{\text{fm}} \stackrel{\text{Paper 1}}{\simeq} \frac{\pi}{3} \alpha \alpha_m \frac{p}{\sqrt{T_\infty T_g^\oplus}} r_0^2 A_1^{\text{fm}} \simeq 2 \Xi \frac{p}{p^*} \tau^{\text{fm}} r_0 J_1 I \quad (50a)$$

$$F_{\text{phot}}^{\text{co}} \stackrel{\text{Eq. 46a}}{=} 4\pi \kappa_s \frac{\eta_{\text{dyn}}^2}{\rho A_0^{\text{co}}} A_1^{\text{co}} = 2 \Xi \frac{p^*}{p} \tau^{\text{co}} r_0 J_1 I, \quad (50b)$$

where the mean scattered gas temperature $\overline{T_g^\oplus}$, the constant Ξ and the characteristic pressure p^* are (like in Rohatschek (1995))

$$\overline{T_g^\oplus} = T_\infty + \alpha (A_0^{\text{fm}} - T_\infty) \quad \text{Eq. A.2}$$

$$A_0^{\text{fm}} \stackrel{\text{Paper 1}}{\equiv} \frac{I J_0 + h T_\infty + \sigma_{\text{SB}} \varepsilon (3(\tilde{T}^{\text{fm}})^4 + T_{\text{rad}}^4)}{h + 4\sigma_{\text{SB}} \varepsilon (\tilde{T}^{\text{fm}})^3} \quad (51a)$$

$$h \stackrel{\text{Paper 1}}{=} \frac{1}{2} \alpha_m \alpha \frac{p}{T_\infty} v_{\text{th}} \quad (51b)$$

$$\Xi = \frac{\pi}{2} \sqrt{\frac{\pi}{3}} \frac{v_{\text{th}} \eta_{\text{dyn}}}{\sqrt{A_0^{\text{co}} \sqrt{T_\infty \overline{T_g^\oplus}}}} \quad (51c)$$

$$p^* = \frac{1}{2} \sqrt{3\pi} \frac{v_{\text{th}} \eta_{\text{dyn}}}{r_0} = \frac{3}{\pi} \Xi \frac{\sqrt{A_0^{\text{co}} \sqrt{T_\infty \overline{T_g^\oplus}}}}{r_0} \quad (51d)$$

$$A_0^{\text{co}} = \frac{I J_0 + \frac{k_g}{r_0} T_\infty + \sigma_{\text{SB}} \varepsilon (3 T_{\text{bb}}^4 + T_{\text{rad}}^4)}{\frac{k_g}{r_0} + 4\sigma_{\text{SB}} \varepsilon T_{\text{bb}}^3}. \quad \text{Eq. 46c}$$

Here, the ideal gas equation $p = \frac{\rho}{M} R_g T_g$ was used to express the mean thermal gas speed as $v_{\text{th}} = \sqrt{8p/(\pi\rho)}$. Eq. 51b is valid for mono-atomic gas, for di-atomic gas the factor 1/2 has

to be replaced with 3/4 (Rohatschek & Zulehner 1985). The mean temperatures \tilde{T}^{fm} and \bar{T} for $h > 0$ can be determined by solving Eq. 51a iteratively with $\tilde{T}^{\text{fm}} = \bar{T}$ starting at T_{bb} . For a relatively small h , $\tilde{T}^{\text{fm}} = T_{\text{bb}}$ (Paper 1). The dimensionless scaling coefficients τ are subsequently

$$\tau^{\text{fm}} = \frac{\sqrt{A_0^{\text{co}}}}{\sqrt[4]{T_\infty T_g^\oplus}} \frac{\alpha \alpha_m}{2} \frac{1}{\frac{k}{r_0} + h + 4\sigma_{\text{SB}}\epsilon (\tilde{T}^{\text{fm}})^3} \quad (52a)$$

$$\tau^{\text{co}} = \frac{\sqrt[4]{T_\infty T_g^\oplus}}{\sqrt{A_0^{\text{co}}}} \kappa_s \frac{1}{\frac{k}{r_0} + 2\frac{k_g}{r_0} + 4\sigma_{\text{SB}}\epsilon T_{\text{bb}}^3}. \quad (52b)$$

The interpolation equation Eq. 49 enables — together with the equations above — to derive

$$\hat{F} = \Xi \sqrt{\tau^{\text{co}} \tau^{\text{fm}}} r_0 J_1 I \quad (53a)$$

$$\hat{p} = \sqrt{\frac{\tau^{\text{co}}}{\tau^{\text{fm}}}} p^*. \quad (53b)$$

Compared to the work in Rohatschek (1995), the maximum force \hat{F} is determined by the geometric mean of τ^{co} and τ^{fm} as additional factor. Similarly, the pressure \hat{p} where the forces maximizes is given by extending the result in Rohatschek (1995) by an additional factor, i.e. the square root of the ratio of the two τ .

5. DISCUSSION

In this section, the underlying *fm* and *co* limit approximations are discussed. A brief comparison to the original model by Rohatschek (1995); Hettner (1928) is given afterwards.

5.1. *fm* limit equation accuracy

In Paper 1 a new approximation for photophoretic forces in the *fm* regime following

$$F_{\text{phot}}^{\text{fm}} \simeq \frac{\pi}{3} \alpha \alpha_m \frac{p}{\sqrt[4]{T_\infty T_g^\oplus}} r_0^2 \frac{I J_1}{\frac{k}{r_0} + h + 4\sigma_{\text{SB}}\epsilon T_{\text{bb}}^3} \quad (54)$$

was introduced. As shown in that paper, this formula for photophoresis on spherical particles with surface temperatures strongly deviating from the gas temperature T_∞ or high intensities I significantly increases the accuracy of analytically determined photophoretic forces with respect to numerical values. Different classic approximation for the photophoretic force in the *fm* regime which are not supporting these gas temperatures and intensity conditions were compared to the new approximation to emphasize the need for an additional equation in the *fm* regime with an extended scope of validity. While still covering the classic scope of validity (for $\alpha_m = 1$, this equation can very well be approximated by the *fm* equation from Beresnev et al. (1993) for $\alpha_n = 1$), Eq. 54 has an average relative error of about 1% for particles with a radius of up to 1.1 mm. With a maximum and minimum relative errors of only 7% and $\approx -50\%$, respectively, (for details see Paper 1), it is far more reliable under rather extreme conditions than the classic *fm* approximations, which then overestimate the force up to orders of magnitude, as they were designed for basically low intensities.

5.2. *co* limit equation accuracy

Table 1: Intervals for the parameter sweep in COMSOL, where the heat transfer equation (Eq. 29a) with the boundary condition given by Eq. 33a was solved ($[a, b]$ denotes an interval between the numbers a and b). All intervals are equally subdivided (log scale; the additional ‘1 m’ for r_0 means, there is a gap between 1 m and 0.11 m concerning this equal subdivision). Details on the subdivision can be found in Loesche (2015).

parameter	parameter sweep intervals
r_0	$[1.1 \times 10^{-4}, 1.1 \times 10^{-1}]$ m, and 1 m
k	$[10^{-3}, 8]$ W m $^{-1}$ K $^{-1}$
I	$[0.5, 40]$ kW m $^{-2}$
T_{rad}	$[0, 350]$ K

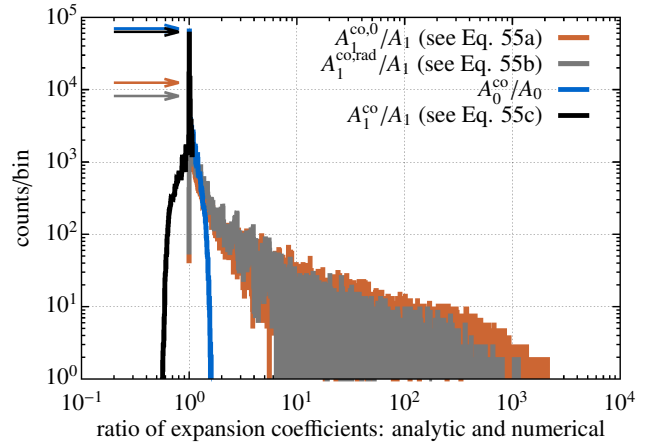


Figure 3: Parameter sweep histogram for 196 344 parameter combinations. The parameter sweep intervals are given in Tab. 1. Like in Paper 1, the effectively exact numerical result was obtained with COMSOL by solving the heat transfer equation (Eq. 29a) with the boundary condition given by Eq. 33a. The bin size is 0.005 (0.5%). Color-coded arrows point towards the respective histogram’s peak. The histogram for A_1^{co} (black) is restricted to $0.57 \leq A_1^{\text{co}}/A_1 \leq 1.07$ while the other expansion coefficients $A_1^{\text{co},0}$ (Reed 1977; Mackowski 1989) and $A_1^{\text{co},\text{rad}}$ are overestimated up to several orders of magnitude. The particle mean temperature A_0^{co} (blue) is also very close to the exact value A_0 , the ratio is within $1.00 \leq A_0^{\text{co}}/A_0 \leq 1.63$.

In this paper, we use the same radiation term in the boundary condition as in the previous paper (see Section 3.3.2). As the force depends on the first expansion coefficient of the gas temperature $C_1^{\text{sf}} \propto A_1^{\text{sf}}$ ($C_1^{\text{co}} = A_1^{\text{co}}$) very close to the surface, a more accurate expansion coefficient A_1 will obviously also improve the quality of the calculated force. This is especially true for high intensities I , where the radiation term $4\sigma_{\text{SB}}\epsilon T_{\text{bb}}^3$ will strongly contribute to the solution. As the description of the entire pressure regimes photophoresis in this paper is based on the interpolation between the *fm* and *co* approximations, only the

Table 2: Statistical properties of the ratio of the particle temperature expansion coefficients (see Eq. 55). A parameter sweep of 196 344 parameter combinations was performed along the parameter intervals given in Tab. 1. Values in round brackets are for r_0 restricted to the interval $[0.11, 11]$ mm.

ratio of particle temperature expansion coefficients: analytic/numerical	min	max	mean	median	STD
$A_1^{\text{co},0}/A_1$	1.00 (1.00)	38 368 (424)	46.9 (7.23)	2.25 (1.35)	357 (20.1)
$A_1^{\text{co,rad}}/A_1$	1.00 (1.00)	20 802 (266)	8.10 (3.00)	1.45 (1.19)	83.2 (7.78)
A_1^{co}/A_1	0.57 (0.66)	1.07 (1.07)	0.97 (0.99)	1.00 (1.00)	0.08 (0.05)
A_0^{co}/A_0	1.00 (1.00)	1.63 (1.43)	1.06 (1.04)	1.01 (1.00)	0.10 (0.07)
$\frac{A_1^{\text{co}}}{A_0^{\text{co}}}/\frac{A_1}{A_0}$	0.35 (0.46)	1.05 (1.05)	0.93 (0.96)	1.00 (1.00)	0.13 (0.10)

thermal radiation contributes as additional term in comparison to Rohatschek (1995), while those boundary conditions which are linear in the Knudsen-number disappear in the *co* limit. We performed a parameter sweep along the values in Tab. 1 and visualize the strong influence of the black body radiation term in the histogram in Fig. 3, where the histograms of each ratio of one of the three expansion coefficients Eq. 55 and its true value are shown. This true value was obtained from temperature distribution across the spheres, calculated with COMSOL. The boundary conditions used in COMSOL are Eq. 33a. Tab. 2 shows minimum and maximum ratios. Beside that, it also shows other distribution information, which does not have a strict mathematical meaning but show a tendency, just as Fig. 3. For simplicity, we restrict ourselves to the *co* limit in this discussion and neglect k_g in the COMSOL calculations, as for gases like air, high intensities and not too small particles the radiation term dominates $2k_g/r_0 \ll 4\sigma_{\text{SB}}\varepsilon T_{\text{bb}}^3$. In the other cases, the consideration of k_g will not prevent any error here but only complicate our considerations, because the term $2\frac{k_g}{r_0}$ in the expansion coefficients did not arise from any linearizations or simplifications in the boundary condition. To investigate the influence of the black body radiation term in the first expansion coefficient of the particle surface temperature A_1 , we therefore either set \tilde{T} to 0, T_∞ and our result T_{bb} :

$$\text{no thermal radiation: } A_1^{\text{co},0} = \frac{I J_1}{\frac{k}{r_0} + 2\frac{k_g}{r_0}} \quad (55a)$$

$$\text{simple thermal rad.: } A_1^{\text{co,rad}} = \frac{I J_1}{\frac{k}{r_0} + 2\frac{k_g}{r_0} + 4\sigma_{\text{SB}}\varepsilon T_{\text{rad}}^3} \quad (55b)$$

$$\text{black body rad.: } A_1^{\text{co,bb}} = \frac{I J_1}{\frac{k}{r_0} + 2\frac{k_g}{r_0} + 4\sigma_{\text{SB}}\varepsilon T_{\text{bb}}^3} \quad (55c)$$

The first equation $A_1^{\text{co},0}$ was obtained by Reed (1977); Mackowski (1989) as they did not include thermal radiation ⁶. The

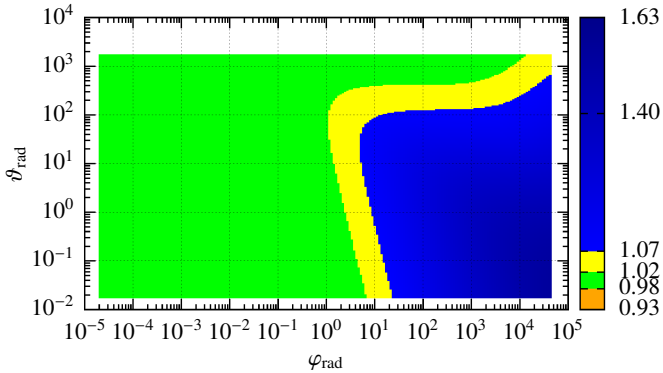
second equation resembles the term used in the *fm* approximation by Beresnev et al. (1993), and the last equation is our previously obtained result (see Eq. 37a). Fig. 3 clearly shows the good performance of $A_1^{\text{co,bb}}$, i.e. when the black body temperature is used. Surprisingly, the coefficient with no radiation $A_1^{\text{co},0}$ and the one that assumes the particle to radiate with T_{rad} both perform equally bad, although $A_1^{\text{co},0}$ with $k_g = 0$ belongs to a boundary condition that does not allow a steady state solution of the heat transfer equation. As in the *co* limit, the photophoretic force depends on $1/\bar{T}$, the histogram of the ratio of the mean temperature $\bar{T} = A_0^{\text{co}}$ and its numerically obtained value is also shown. It is mirrored at the ratio 1. In Paper 1 it was shown, that these two dimensionless variables

$$\varphi_{\text{rad}} = \frac{\varepsilon I_0 r_0}{k T_{\text{rad}}} \quad (56a)$$

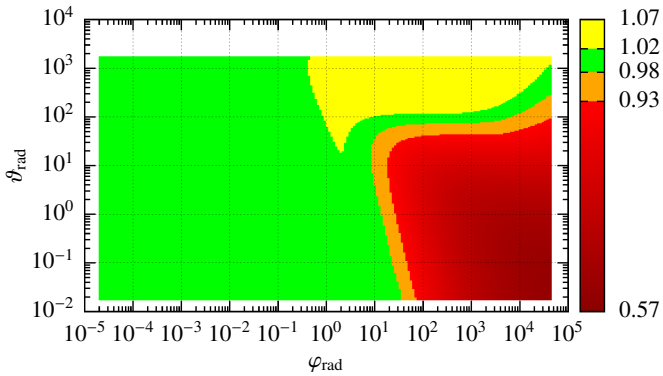
$$\vartheta_{\text{rad}} = \sigma_{\text{SB}} \frac{T_{\text{rad}}^4}{I_0} \quad (56b)$$

characterize different results of the heat transfer problem (scaled to unit sphere; here for omitted k_g). In Fig. 4 the ratio of A_0^{co} and A_1^{co} to their respective exact numerical values are plotted over φ_{rad} and ϑ_{rad} . From the plots one can conclude, that in the given parameter range (see Tab. 1), the relative error of A_0^{co} and A_1^{co} is less than 2% for $\varphi_{\text{rad}} < 1$. Within the model, the results in Eq. 46 carry about the same error.

⁶Reed (1977): $J_1 = 1/2$ here



(a) A_0^{co}/A_0



(b) A_1^{co}/A_1

Figure 4: Ratio of the particle temperature expansion coefficients. The dimensionless variables φ_{rad} and ϑ_{rad} are defined in Eq. 56. The plot for $\frac{A_1^{\text{co}}/A_1}{A_0^{\text{co}}/A_0}$ is very similar to Fig. 4b, basically only varying in the bounds of the ratio: $0.35 \leq \frac{A_1^{\text{co}}/A_1}{A_0^{\text{co}}/A_0} \leq 1.05$, therefore we refrain from plotting this.

5.3. Changes for the entire range of pressures

As the *fm* approximation shows even smaller relative errors for the same parameter sweep (Paper 1), the interpolation is based on two robust equations, that are the *fm* and *co* limit approximation of the photophoretic force.

In the following we discuss the predictions of this model for the entire range of pressures and compare them to those made

in Rohatschek (1995):

$$\hat{F}_R = \Xi_R \sqrt{\kappa_s \frac{\alpha r_0}{2k}} r_0 J_1 I \quad (57a)$$

$$\hat{p}_R = \sqrt{\kappa_s \frac{2}{\alpha}} p^* \quad (57b)$$

$$\Xi_R = \frac{\pi}{2} \sqrt{\frac{\pi}{3}} \frac{v_{\text{th}} \eta_{\text{dyn}}}{T_\infty} \quad (57c)$$

$$p^* = \frac{1}{2} \sqrt{3\pi} \frac{v_{\text{th}} \eta_{\text{dyn}}}{r_0} \quad (57d)$$

Just as the underlying *fm* and *co* approximations for the interpolation model in Rohatschek (1995), the model is also assuming very low deviances from gas and mean surface temperature. Additionally, for simplicity, Rohatschek (1995) omitted k_g in $A_1^{\text{co},0} = \frac{I J_1}{\frac{k}{r_0} + 2 \frac{k_g}{r_0}}$ (Eq. 55a) in his model so that $A_1^{\text{co},0}$ is equal to $A_1^{\text{fm},0} = r_0 \frac{I J_1}{k}$ ($h = 0$, too). For very low gas heat conductivities k_g such as air this will not introduce a significant error, but for hydrogen-helium gases it will. Beside that, the introduced error will grow strongly as the discussed particles get larger (see Paper 1). In our model this is not the case anymore. But for low intensities I and low gas heat conductivity k_g , the interpolation proposed in this paper is basically the same as in Rohatschek (1995), which performs well (see Rohatschek (1995) and Sec. 4) within its scope. We calculated the changes of \hat{F} and \hat{p} with respect to the values obtained with the model from Rohatschek (1995) (\hat{F}_R and \hat{p}_R). For extreme values, the force ratio \hat{F}/\hat{F}_R can reach values between $2.7 \cdot 10^{-5}$ and 2.7. The minimum pressure ratio \hat{p}/\hat{p}_R can be as low as 0.13, the maximum one 1.8. Fig. 5 shows photophoretic forces for these extreme values as well as two more realistic cases in comparison to the predictions made in Rohatschek (1995). The corresponding parameters and values are listed in Tab. 3. We chose a laser illuminated mm-sized particle in a cooled experimental setup and a particle in an astrophysical context as example studies which results in force/pressure ratios of $\hat{F}/\hat{F}_R = 0.34$ with $\hat{p}/\hat{p}_R = 0.72$, and $\hat{F}/\hat{F}_R = 0.17$ with $\hat{p}/\hat{p}_R = 0.15$, respectively. Both values — especially in the last case — show significantly different predictions. However, experimental investigations on the interpolation for high intensities are subject to future work at this moment and beyond the scope of this paper. One should mention here that rotation of illuminated particles — which are observed especially in experimental studies e.g. by van Eymeren & Wurm (2012) — have high influence on the photophoretic force (Loesche et al. 2014).

As for high I the temperature-dependence of k_g and η_{dyn} can be important, the mean temperature Eq. 46c can be iteratively calculated if $k_g = k_g(T)$. Then, the force in the *co* limit $F^{\text{co}} = F^{\text{co}}(k(\bar{T}), k_g(\bar{T}), \eta_{\text{dyn}}(\bar{T}))$ with $\bar{T} = A_0^{\text{co}}$ can be obtained. In the *fm* regime, the mean temperature Eq. 51a determines the heat conductivity $k = k(\bar{T} = A_0^{\text{fm}})$, and therefore the force.

6. CONCLUSION

In the model introduced in Paper 1 (Loesche et al. 2016) as well as here we incorporate possible temperature differences

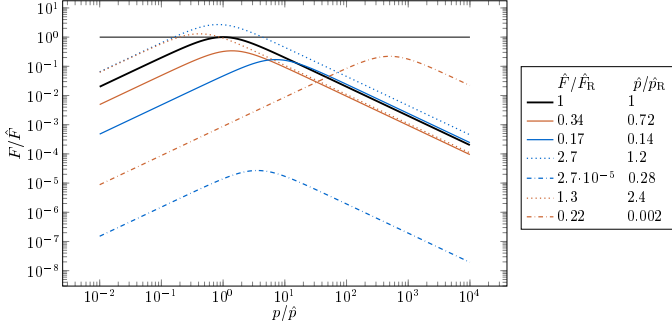


Figure 5: Two case studies as well as the maximum alteration of the interpolation model $F_{\text{phot}} = F_{\text{phot}}(\hat{F}, \hat{p})$ with respect to the model in Rohatschek (1995) along Tab. 3.

between the illuminated object and the surrounding gas. This also includes the case of higher radiative fluxes I . The solutions for the free molecule regime (Paper 1) and the slip flow regime (Eq. 44) can be calculated using the given formulae. The usage of the interpolation between the *fm* and *co* regimes is more complicated. The basic approximation in this paper follows (for simplicity, omitting h)

$$F_{\text{phot}} = \frac{2\hat{F}}{\frac{p}{\hat{p}} + \frac{\hat{p}}{p}}$$

$$\hat{F} = \frac{\pi}{2} \sqrt{\frac{\pi}{3}} \frac{v_{\text{th}} \eta_{\text{dyn}}}{\sqrt{A_0^{\text{co}} \sqrt{T_{\infty} T_{\text{g}}^{\oplus}}}} \sqrt{\tau^{\text{co}} \tau^{\text{fm}}} r_0 J_1 I$$

$$\hat{p} = \sqrt{\frac{\tau^{\text{co}}}{\tau^{\text{fm}}}} \frac{1}{2} \sqrt{3\pi} \frac{v_{\text{th}} \eta_{\text{dyn}}}{r_0}$$

with the mean thermal speed of the gas

$$v_{\text{th}} = \sqrt{\frac{8p}{\pi\rho}}$$

and the mean temperatures

$$A_0^{\text{co}} = \frac{I J_0 + \frac{k_{\text{g}}}{r_0} T_{\infty} + \sigma_{\text{SB}} \varepsilon (3T_{\text{bb}}^4 + T_{\text{rad}}^4)}{\frac{k_{\text{g}}}{r_0} + 4\sigma_{\text{SB}} \varepsilon T_{\text{bb}}^3}$$

$$\overline{T_{\text{g}}^{\oplus}} = T_{\infty} + \alpha \left(\frac{I J_0 + \sigma_{\text{SB}} \varepsilon (3T_{\text{bb}}^4 + T_{\text{rad}}^4)}{4\sigma_{\text{SB}} \varepsilon T_{\text{bb}}^3} - T_{\infty} \right)$$

and the scaling factors

$$\tau^{\text{fm}} = \frac{\sqrt{A_0^{\text{co}}}}{\sqrt[4]{T_{\infty} T_{\text{g}}^{\oplus}}} \frac{\alpha \alpha_{\text{m}}}{2} \frac{1}{\frac{k}{r_0} + 4\sigma_{\text{SB}} \varepsilon T_{\text{bb}}^3}$$

$$\tau^{\text{co}} = \frac{\sqrt[4]{T_{\infty} T_{\text{g}}^{\oplus}}}{\sqrt{A_0^{\text{co}}}} \kappa_{\text{s}} \frac{1}{\frac{k}{r_0} + 2\frac{k_{\text{g}}}{r_0} + 4\sigma_{\text{SB}} \varepsilon T_{\text{bb}}^3}.$$

The importance of this model considering strong temperature deviations and high intensities for longitudinal photophoresis

becomes apparent when calculating drift motion of dust particles in a (pre-)transitional protoplanetary disk, where the mean free path of the gas is often in the same order as the particles diameters. Especially near the central star the temperatures of the illuminated particles can get significantly higher than the temperature of the surrounding gas. Since photophoresis can dominate the force balance for small particles, the accuracy of the approximation used is highly important and therefore the model given in this paper has to be favored. Also, particles illuminated with lasers (Daun et al. 2008; Loesche et al. 2014) can lead to rather extreme conditions, previously not supported by approximations for the *fm* and transition regimes.

7. ACKNOWLEDGMENTS

C.L. was funded by DFG 1385. T.H. was funded by the DFG under the grant number WU321/12-1.

A. SUPPLEMENTARIES

A.1. One orthogonality relation for associated Legendre polynomials

$$\int_{-1}^{-1} P_{\nu}^{\mu}(x) P_{\psi}^{\mu}(x) dx = \delta_{\nu\psi} \frac{2}{2\nu+1} \frac{(\nu+\mu)!}{(\nu-\mu)!} \quad (\text{A.1})$$

A.2. Average

The mean temperature of the scattered gas T_{g}^{\oplus} (*fm*, see Paper 1) is (with α denoting the thermal accommodation coefficient)

$$\overline{T_{\text{g}}^{\oplus}} = T_{\infty} + \alpha (\overline{T} - T_{\infty}). \quad (\text{A.2})$$

A.3. Transport numbers

$$Pe = Re Pr = \frac{\rho c_p u l}{k} \quad (\text{A.3})$$

$$Re = \frac{\rho u l}{\eta_{\text{dyn}}} \quad (\text{A.4})$$

$$Pr = \frac{c_p}{k} \eta_{\text{dyn}} \quad (\text{A.5})$$

A.4. Force

The force exerted onto the suspended particle is given by

$$\mathbf{F} = \int_{\partial V} \underline{\Pi} \cdot d\mathbf{A} \quad (\text{A.6a})$$

$$\underline{\Pi} = -\rho \mathbf{v} \otimes \mathbf{v} + \underline{\sigma}. \quad (\text{A.6b})$$

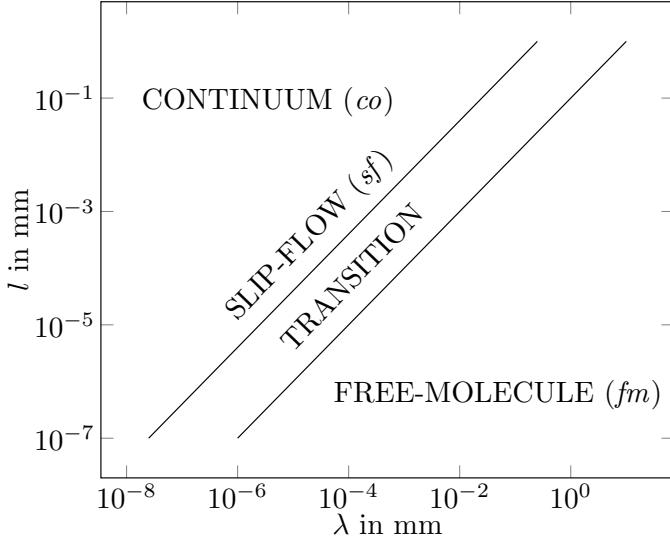


Figure A.6: Knudsen regimes. The Knudsen number is defined as $Kn = \lambda l^{-1}$.

Here, due to the symmetry of the problem, only F_z is not zero. As it is $d\mathbf{A} \equiv \mathbf{n} dA$ where $\mathbf{n} = \mathbf{e}_r$ is the normal vector, the product $\underline{\Pi} \cdot \mathbf{n}$ has to be determined

$$\underline{\Pi} \cdot \mathbf{n} = \underline{\Pi} \cdot \mathbf{e}_r \quad (\text{A.7a})$$

$$= \begin{pmatrix} \Pi_{rr} & \Pi_{r\zeta} & \Pi_{r\xi} \\ \Pi_{\zeta r} & \Pi_{\zeta\zeta} & \Pi_{\zeta\xi} \\ \Pi_{\xi r} & \Pi_{\xi\zeta} & \Pi_{\xi\xi} \end{pmatrix} \cdot \begin{pmatrix} 1 \\ 0 \\ 0 \end{pmatrix} \quad (\text{A.7b})$$

$$= \begin{pmatrix} \Pi_{rr} \\ \Pi_{\zeta r} \\ \Pi_{\xi r} \end{pmatrix} = \Pi_{rr} \mathbf{e}_r + \Pi_{\zeta r} \mathbf{e}_\zeta + \Pi_{\xi r} \mathbf{e}_\xi. \quad (\text{A.7c})$$

As $\underline{\Pi}$ is given by Eqs. A.6b and 6, the respective parts in spherical coordinates, and with incompressibility are

$$R_{rr} = 2\eta_{\text{dyn}} \frac{\partial v_r}{\partial r} \quad (\text{A.8a})$$

$$R_{\zeta r} = \eta_{\text{dyn}} \left(\frac{1}{r} \frac{\partial v_r}{\partial \zeta} + r \frac{\partial}{\partial r} \left(\frac{v_\zeta}{r} \right) \right) \quad (\text{A.8b})$$

$$\Pi_{rr} \stackrel{\text{Eq. A.8a}}{=} -\rho v_r^2 - p + 2\eta_{\text{dyn}} \partial_r v_r \quad (\text{A.8c})$$

$$\Pi_{\zeta r} \stackrel{\text{Eq. 16}}{=} -\rho v_\zeta v_r + \eta_{\text{dyn}} \left(\frac{1}{r} \partial_\zeta v_r + r \partial_r \left(\frac{v_\zeta}{r} \right) \right) \quad (\text{A.8d})$$

$$\Pi_{\xi r} = 0. \quad (\text{A.8e})$$

$\Pi_{\xi r} = 0$ as $v_\xi = 0$, and \mathbf{v} is independent of ξ . The z -component of the product in Eq. A.7 is

$$(\underline{\Pi} \cdot \mathbf{n})_z = \Pi_{rr} \cos \zeta - \Pi_{\zeta r} \sin \zeta, \quad (\text{A.9})$$

and therefore the z -component of the force (Eq. A.6a) reads

$$F_z = 2\pi r_0^2 \int_0^\pi d\zeta \sin \zeta \left(\Pi_{rr} \cos \zeta - \Pi_{\zeta r} \sin \zeta \right). \quad (\text{A.10})$$

Table A.4: Notation.

variable	meaning
$\mathbf{r} = (r, \zeta, \xi)$	spherical coordinates (Fig. 1)
r_0	radius of spherical particle suspended in gas
\mathbf{n}, \mathbf{t}	normal and tangent vectors of a surface
∂V	border of the volume V , i.e. $r = r_0$ for the sphere
\mathbf{v}	gas mass velocity in m s^{-1}
v_{th}	mean thermal gas speed
\mathbf{u}	velocity of the suspended particle, relative to the gas
$T(r, \zeta, \xi)$	particle temperature in K
\bar{T}, \bar{T}	mean particle surface temperatures in K (Eqs. 38 and 35)
T_g	gas temperature
T_∞	gas temperature far away from the particle
$T_g^{\oplus/\ominus}$	gas temperature for velocity half-spaces $\mathbf{n} \cdot \mathbf{v} > 0$ and $\mathbf{n} \cdot \mathbf{v} < 0$ (Fig. 1), used in the <i>fm</i> regime (see Paper 1), here we write $T_g^\ominus = T_\infty$
$\overline{T_g _{\partial V}}$	mean temperature of the gas layer around the particle
T_{rad}	temperature of external radiation field
T_{bb}	black-body temperature (Eq. 43)
R_g	universal gas constant in $\text{J mol}^{-1} \text{K}^{-1}$
M	molar gas mass in kg mol^{-1}
p	gas pressure in Pa
\hat{p}	gas pressure where \mathbf{F}_{phot} maximizes (Eq. 53b)
p^*	characteristic gas pressure (Eq. 51d)
ρ	gas mass density in kg m^{-3}
$\underline{\sigma}, \underline{R}$	stress and friction tensor (Eq. 6)
ψ	stream function
E^2	stream function operator (Eq. 10b)
P_v^μ	associated Legendre polynomial
\mathbf{F}_{phot}	photophoretic force
\hat{F}	maximum photophoretic force at a pressure \hat{p} (Eq. 53a)
δ	stretch factor in Eq. 48
$\tau^{\text{fm}}, \tau^{\text{co}}$	dimensionless scaling coefficients for \hat{F} and \hat{p} (Eq. 52)
Ξ	scaling constant for \hat{F} and \hat{p} in Pa m K^{-1} (Eq. 51c)
$\varphi_{\text{rad}}, \vartheta_{\text{rad}}$	dimensionless solution numbers (Eq. 56)
α, α_m	thermal and momentum accommodation coefficient (dimensionless)
κ_t	temperature jump coefficient (dimensionless), related to α (Eq. 36)
κ_m	gas-kinetic frictional slip (or momentum exchange) coefficient (dimensionless), related to α_m
κ_h	thermal stress slip coefficient (dimensionless)
κ_s	thermal creep (or thermal slip) coefficient (dimensionless), related to α_m (Eq. 4)

J_v	asymmetry factor (dimensionless, Eq. 32)
k	thermal conductivity of suspended particle in $\text{W m}^{-1} \text{K}^{-1}$
k_g	thermal conductivity of the gas
$\eta_{\text{kin}}, \eta_{\text{dyn}}$	kinematic and dynamic viscosity, $\eta_{\text{kin}} = \eta_{\text{dyn}}/\rho$, η_{dyn} in Pa s
Pe	Péclet number (Eq. A.3)
Re	Reynolds number (Eq. A.4)
Pr	Prandtl number (Eq. A.5)
h	heat transfer coefficient (Eq. 51b) in $\text{W m}^{-2} \text{K}^{-1}$
I	effective intensity $I = \varepsilon I_0$ in W m^{-1}
ε	(mean) emissivity
σ_{SB}	Stefan-Boltzmann constant in $\text{W m}^{-2} \text{K}^{-4}$
λ	mean free path of the gas in m
Kn	Knudsen number (dimensionless, Eq. 1)
q	normalized source function (Eq. 29) in m^{-1}
$A_\nu, B_\nu, C_\nu, q_\nu$	expansion coefficients ($\nu \geq 0$)

Table 3: Changes of \hat{F} and \hat{p} with respect to the values obtained with the model from Rohatschek (1995). Extreme situations as well as two example studies are also sketched in Fig. 5.

	I	k	r_0	k_g	T_∞	T_{rad}	\hat{F}/\hat{F}_R	\hat{p}/\hat{p}_R
in	W m^{-2}	$\text{W m}^{-1} \text{K}^{-1}$	m	$\text{W m}^{-1} \text{K}^{-1}$	K	K		
CASE I:	10^4	1	10^{-3}	$2 \cdot 10^{-2}$	70	70	0.34	0.72
CASE II:	10^3	10^{-2}	10^{-4}	0.2	500	3	0.17	0.14
MAX(\hat{F}/F_R)	520	8	$1.1 \cdot 10^{-3}$	10^{-3}	1500	250	2.7	1.2
MIN(\hat{F}/F_R)	$4 \cdot 10^4$	10^{-3}	$1.1 \cdot 10^{-3}$	$2 \cdot 10^{-2}$	10	1500	$2.7 \cdot 10^{-5}$	0.28
MAX(\hat{p}/p_R)	6900	8	$1.1 \cdot 10^{-3}$	10^{-3}	1500	1	1.3	2.4
MIN(\hat{p}/p_R)	10	10^{-3}	$8.7 \cdot 10^{-6}$	$2 \cdot 10^{-2}$	10	1500	0.22	$2 \cdot 10^{-3}$

References

References

- Arnold, S., & Amani, Y. (1980). Broadband photophoretic spectroscopy. *Optics Letters*, 5, 242–244. doi:10.1364/OL.5.000242.
- Bakanov, S. (2004). The nature of thermophoresis of highly heat-conducting bodies in gases. *Journal of Applied Mathematics and Mechanics*, 68, 25–28. doi:10.1016/S0021-8928(04)90002-0.
- Bakanov, S. P. (1992). Thermophoresis in gases at small Knudsen numbers. *Soviet Physics Uspekhi*, 35, 783–792. URL: <http://stacks.iop.org/0038-5670/35/i=9/a=A03>. doi:10.1070/PU1992v035n09ABEH002263.
- Beresnev, S., Chernyak, V., & Fomyagin, G. (1993). Photophoresis of a spherical particle in a rarefied gas. *Physics of Fluids*, 5, 2043–2052. doi:10.1063/1.858540.
- Brenner, H. (2005). Nonisothermal Brownian motion: Thermophoresis as the macroscopic manifestation of thermally biased molecular motion. *Phys. Rev. E*, 72, 061201. doi:10.1103/PhysRevE.72.061201.
- Brenner, H. (2006). Elementary kinematical model of thermal diffusion in liquids and gases. *Phys. Rev. E*, 74, 036306. doi:10.1103/PhysRevE.74.036306.
- Brenner, H. (2009). A nonmolecular derivation of Maxwell's thermal-creep boundary condition in gases and liquids via application of the LeChatelier-Braun principle to Maxwell's thermal stress. *Physics of Fluids*, 21, 053602. doi:10.1063/1.3139273.
- Chang, Y. C., & Keh, H. J. (2012). Effects of thermal stress slip on thermophoresis and photophoresis. *Journal of Aerosol Science*, 50, 1–10. URL: <http://www.sciencedirect.com/science/article/pii/S0021850212000584>. doi:10.1016/j.jaerosci.2012.03.006.
- Chernyak, V. G., & Beresnev, S. A. (1993). Photophoresis of aerosol particles. *Journal of Aerosol Science*, 24, 857–866. doi:10.1016/0021-8502(93)90066-I.
- Daun, K. J., Smallwood, G. J., & Liu, F. (2008). Investigation of Thermal Accommodation Coefficients in Time-Resolved Laser-Induced Incandescence. *J. Heat Transfer*, 130, 121201. doi:10.1115/1.2977549.
- van Eymeren, J., & Wurm, G. (2012). The implications of particle rotation on the effect of photophoresis. *MNRAS*, 420, 183–186. doi:10.1111/j.1365-2966.2011.20020.x.
- Happel, J., & Brenner, H. (1983). *Low Reynolds number hydrodynamics: with special applications to particulate media* volume 1. Springer. doi:10.1007/978-94-009-8352-6.
- Hesse, A. (2011). *Mikrogravitations- und Laborexperimente zur Bestimmung photophoretischer Kräfte auf extraterrestrische Materialien*. Master's thesis Universität Duisburg-Essen.
- Hettner, G. (1928). Neuere experimentelle und theoretische Untersuchungen über die Radiometerkräfte. *Ergebnisse der exakten Naturwissenschaften*, 7, 209–237. doi:10.1007/BFb0111851.
- Hidy, G. M., & Brock, J. R. (1967). Photophoresis and the Descent of Particles into the Lower Stratosphere. *J. Geophys. Res.*, 72, 455–460. doi:10.1029/JZ072i002p00455.
- Hidy, G. M., & Brock, J. R. (Eds.) (1970). *The Dynamics of Aerocolloidal Systems* volume 1 of *International Reviews in Aerosol Physics and Chemistry*. (1st ed.). Pergamon Press, Oxford.
- Ivchenko, I. N., Loyalka, S. K., & Tompson, R. V. (1993). A boundary model for the thermal creep problem. *Fluid Dynamics*, 28, 876–878. doi:10.1007/BF01049795.
- Ivchenko, I. N., Loyalka, S. K., & Tompson, R. V. (2007). *Analytical methods for problems of molecular transport* volume 83 of *Fluid Mechanics and Its Applications*. Springer.
- Loesche, C. (2015). *On the photophoretic force exerted on mm- and sub-mm-sized particles*. Ph.D. thesis Universität Duisburg-Essen.
- Loesche, C., Teiser, J., Wurm, G., Hesse, A., Friedrich, J. M., & Bischoff, A. (2014). Photophoretic Strength on Chondrules. 2. Experiment. *ApJ*, 792, 73. doi:10.1088/0004-637X/792/1/73.
- Loesche, C., Wurm, G., Jankowski, T., & Kuepper, M. (2016). Photophoresis on particles hotter/colder than the ambient gas in the free molecular flow. *Journal of Aerosol Science*, 97, 22–33. doi:10.1016/j.jaerosci.2016.04.001.
- Loesche, C., Wurm, G., Teiser, J., Friedrich, J. M., & Bischoff, A. (2013). Photophoretic Strength on Chondrules. 1. Modeling. *ApJ*, 778, 101. URL: <http://stacks.iop.org/0004-637X/778/i=2/a=101>. doi:10.1088/0004-637X/778/2/101.
- Mackowski, D. W. (1989). Photophoresis of aerosol particles in the free molecular and slip-flow regimes. *International Journal of Heat and Mass Transfer*, 32, 843–854. URL: <http://www.sciencedirect.com/science/article/pii/0017931089902330>. doi:10.1016/0017-9310(89)90233-0.
- Malai, N. V., Limanskaya, A. V., Shchukin, E. R., & Stukalov, A. A. (2012a). Photophoresis of heated large spherical aerosol particles. *Journal of Technical Physics*, 57, 1364–1371. doi:10.1134/S1063784212100131.
- Malai, N. V., Limanskaya, A. V., Shchukin, E. R., & Stukalov, A. A. (2012b). Photophoresis of heated moderately large spherical aerosol particles. *Atmospheric and Oceanic Optics*, 5, 355–363. doi:10.1134/S1024856012050065.
- Maxwell, J. C. (1879). On stresses in rarified gases arising from inequalities of temperature. *Philosophical Transactions of the Royal Society of London*, 170, 231–256.
- Reed, L. D. (1977). Low knudsen number photophoresis. *Journal of Aerosol Science*, 8, 123–131. URL: <http://www.sciencedirect.com/science/article/pii/0021850277900738>. doi:10.1016/0021-8502(77)90073-8.
- Rohatschek, H. (1985). Direction, magnitude and causes of photophoretic forces. *Journal of Aerosol Science*, 16, 29–42. URL: <http://www.sciencedirect.com/science/article/pii/0021850285900187>. doi:10.1016/0021-8502(85)90018-7.
- Rohatschek, H. (1995). Semi-empirical model of photophoretic forces for the entire range of pressures. *Journal of Aerosol Science*, 26, 717–734. URL: <http://www.sciencedirect.com/science/article/pii/002185029500011Z>. doi:10.1016/0021-8502(95)00011-Z.
- Rohatschek, H., & Zulehner, W. (1985). The photophoretic force on nonspherical particles. *Journal of Colloid and Interface Science*, 108, 457–461. URL: <http://www.sciencedirect.com/science/article/pii/0021979785902851>. doi:10.1016/0021-9797(85)90285-1.
- Rosen, M. H., & Orr, C., Jr. (1964). The photophoretic force. *Journal of Colloid Science*, 19, 50–60. URL: <http://www.sciencedirect.com/science/article/pii/0095852264900066>. doi:10.1016/0095-8522(64)90006-6.
- Schubert, G. (Ed.) (2015). *Treatise on Geophysics*. Elsevier.
- Tong, N. T. (1973). Photophoretic force in the free molecule and transition regimes. *Journal of Colloid and Interface Science*, 43, 78–84. doi:10.1016/0021-9797(73)90349-4.
- Tong, N. T. (1975). Experiments on photophoresis and thermophoresis. *Journal of Colloid and Interface Science*, 51, 143–151. doi:10.1016/0021-9797(75)90091-0.
- Wurm, G., & Krauss, O. (2008). Experiments on negative photophoresis and application to the atmosphere. *Atmospheric Environment*, 42, 2682–2690. doi:10.1016/j.atmosenv.2007.07.009.
- Yalamov, Y. I., Kutukov, V. B., & Shchukin, E. R. (1976a). Motion of small aerosol particle in a light field. *Journal of Engineering Physics*, 30, 648–652. doi:10.1007/BF00859364.
- Yalamov, Y. I., Kutukov, V. B., & Shchukin, E. R. (1976b). Theory of the photophoretic motion of the large-size volatile aerosol particle. *Journal of Colloid and Interface Science*, 57, 564–571. URL: <http://www.sciencedirect.com/science/article/pii/0021979776902344>. doi:10.1016/0021-9797(76)90234-4.